

On DDO 154 and Cold Dark Matter halo profiles

Sergio Gelato and Jesper Sommer-Larsen

Theoretical Astrophysics Center, Juliane Maries Vej 30, 2100 Copenhagen Ø, Denmark

1 January 2018

ABSTRACT

We investigate the claim by Burkert and Silk (1997) that the observed rotation curve of the dwarf irregular galaxy DDO 154 cannot be reconciled with the universal CDM halo profile of Navarro, Frenk & White (1996a; 1997) even when allowance is made for the effect of violent gas outflow events on the structure of the galaxy. By means of N -body simulations we show that under certain conditions it is possible to obtain a reasonable fit to the observed rotation curve without invoking Burkert & Silk’s proposed spheroidal MACHO component. We are able to best reproduce the observed decline in the rotation curve by postulating additional hidden disc mass, in an amount that is compatible with disc stability requirements. In the process we improve upon the results of Navarro, Eke & Frenk (1996b) on the formation of halo cores by mass loss by using actual haloes from Cold Dark Matter simulations instead of Hernquist (1990) distributions.

Key words: methods: numerical – galaxies: kinematics and dynamics – galaxies: individual: DDO 154 – galaxies: structure – galaxies: formation – galaxies: haloes

1 INTRODUCTION

A rather generic feature of N -body models of collisionless gravitational collapse is the presence of a central density cusp in the objects that result. While such cusps are observed in many elliptical galaxies, and while in large high-surface-brightness spirals the dominant disc component makes them difficult to discern unambiguously, they are conspicuously absent from the profiles one infers from the observed rotation curves of dwarf disc galaxies (Moore 1994; Flores & Primack 1994). Instead, the dynamics of these objects imply a dark matter distribution characterized by an extended core of nearly uniform density. The nearby galaxy DDO 154 is a prime example: Carignan & Freeman (1988) find a well-constrained fit of the dark matter component by an isothermal sphere with a core radius $r_c = 3.0$ kpc.

Navarro, Eke and Frenk (1996b, hereafter NEF) have shown how the central cusp could have been erased some time after the halo was assembled, by the violent relaxation that follows a sudden large, presumably starburst-driven, mass ejection event. In their numerical N -body experiments they added a slowly growing disc potential to the halo, then removed it abruptly. The slow growth of the disc causes the inner parts of the halo to contract adiabatically, and increases the velocity dispersion there. The subsequent sudden mass loss reduces the binding energy in the central region, leading on a dynamical time scale to the establishment of a new equilibrium with a core in the density profile.

NEF assumed a Hernquist (1990) distribution function for the halo at the beginning of the disc growth phase. This

distribution has a weak ($\rho \propto r^{-1}$) central cusp similar to that reported by Dubinski & Carlberg (1991) and consistent with the “universal halo profile” of Navarro, Frenk & White (1996a; 1997, hereafter collectively NFW). The density profile of the Hernquist distribution falls off more quickly (as r^{-4} rather than r^{-3}) at large radii, however; this difference has a bearing on the behaviour of the rotation curve at large galactocentric distances (which was not the focus of NEF’s study) and also affects the velocity structure within the halo. Perhaps more importantly, the universality of r^{-1} cusps in CDM haloes is somewhat controversial: various groups (Fukushige & Makino 1997; Moore et al. 1997) report steeper slopes in higher-resolution simulations with finer mass granularity. These stronger cusps are naturally more difficult to obliterate (see our results below).

NFW claim that in a wide range of Cold Dark Matter (CDM) cosmogonies the radial profiles of virialised haloes are well described by

$$\rho(r) = \frac{\delta_c \rho_c r_s^3}{r(r_s + r)^2} \quad (1)$$

where ρ_c is the mean density of the Universe, δ_c a characteristic density enhancement, and r_s a characteristic radius around which the profile changes from a logarithmic slope of -1 to one of -3 . For a halo of a given mass M_{200} within the virial radius r_{200} (which, following common practice, we define as the radius of a sphere within which the mean density is $200\rho_c$), δ_c is related to the “concentration parameter” $c \equiv r_{200}/r_s$ by

arXiv:astro-ph/9806289v2 22 Oct 1998

$$\delta_c = \frac{200}{3} \frac{c^3}{[\ln(1+c) - c/(1+c)]}. \quad (2)$$

Since in a CDM cosmogony haloes of a given mass are preferentially assembled in a fairly narrow range of redshifts (with smaller haloes forming first), there is a correlation between δ_c (or c) and M_{200} : less massive haloes are denser and more centrally concentrated.

In the case of DDO 154, a very isolated dwarf disc galaxy whose HI rotation curve has been measured to a considerable distance from its centre (Carignan & Freeman 1988; Hoffman et al. 1993), the “universal profile” of NFW cannot simultaneously account for the observations at small and at large radii. If the parameters (δ_c , r_s) are chosen to fit the observations at small radii (after allowance has been made for the formation of a uniform-density core by mass outflow), the NFW profile predicts that the rotation curve should continue to rise well beyond the radius at which it is observed to peak. If on the other hand the parameters are adjusted to fit the declining part of the rotation curve, the NFW profile predicts an unreasonably large mass excess in the central regions. Burkert & Silk (1997, hereafter BS) have invoked this difficulty as an argument for the presence of an additional dark component formed through dissipative processes, analogous to the putative MACHO component of our own Galaxy. In their view, this new component should be spheroidal rather than disc-like since an overly massive disc would be unstable to fragmentation and expected to form large quantities of stars, contrary to what is observed in this galaxy. They still assume that before this dissipational collapse process the halo was well described by the NFW profile.

DDO 154 is not the only dwarf galaxy for which the observational data are at variance with the cuspy profiles predicted by most N -body simulations. Burkert (1995) and Kravtsov et al (1998) have argued that the observational data can be described by a different one-parameter family of profiles with at most a very weak cusp. Of the galaxies examined in these two works, however, only DDO 154 and NGC 2915 have the very extended rotation curves required for a really stringent test of secular evolution models for the halo density profile. NGC 2915 (Meurer et al. 1996) is in many ways a peculiar object, making it much more difficult to model. We therefore follow the example of Burkert & Silk (1997) and concentrate on DDO 154 alone.

In this paper we explore the possibility of achieving a reasonable fit to the observed rotation curve of DDO 154 without invoking such a dissipative spheroidal component. Instead, we experiment with different mass ejection fractions and disc density distributions. We improve on the work of NEF by using halo distribution functions drawn from ab initio cosmological simulations: the Hernquist (1990) distribution’s unrealistically fast drop-off at large radii might yield a spuriously better fit to the falling part of the rotation curve. Also, NEF’s preferred fits for DDO 154 involve characteristic scale lengths (a_h in their notation, corresponding roughly to r_s in this paper) an order of magnitude larger than expected for the halo of DDO 154 if one assumes a total mass of order $10^{10} M_\odot$ or less, commensurate with the observed radial extent and rotation velocity of this galaxy. (A larger total mass would likely only exacerbate the difficulty in reproducing the observed decline in the rotation

curve.) Alternatively, NEF’s disc scale lengths are unreasonably small (1–4%) by comparison to the halo scale length. In the present work, by contrast, the characteristic halo radius r_s is determined by our ab initio cosmological simulations, and is in good agreement with the results of NFW; our disc scale lengths are also based on observations.

We study both models in which the present-day disc mass is as implied by optical and HI observations of DDO 154 (Carignan & Freeman 1988) and models with additional baryonic mass. In the latter case, the additional mass is assumed to be hidden in some hitherto undetected form and distributed like the observed HI. (The mean metallicity of DDO 154, as measured by the O/H abundance ratio, is only $0.05 Z_\odot$ (van Zee, Haynes & Salzer 1997), and at such a low metallicity there are both theoretical (Maloney & Black 1988) and observational (Verter & Hodge 1995) indications that the CO-to-H₂ conversion ratio should be very large, implying that significant amounts of H₂ could be present without conspicuous associated CO emission.) We examine the argument that a more massive disc would be Toomre-unstable and form stars at a higher rate than observed, and find that we can accommodate a disc up to three times more massive than reported from HI observations without having to assume an implausibly strong stabilizing pressure within the disc.

Section 2 describes in detail the parameters of our N -body simulations. Results are presented in section 3, and conclusions drawn in section 4.

2 THE SIMULATIONS

2.1 Initial conditions

We selected initial conditions out of a realization of a standard CDM power spectrum ($\Omega = 1$, $\Lambda = 0$, $h \equiv H_0/(100 \text{ km s}^{-1} \text{ Mpc}^{-1}) = 0.5$) normalized to $\sigma_8 = 0.6$. This realization was computed on a 128^3 grid in a periodic box of only $4h^{-1}$ Mpc on a side; this would be too small for studies of clustering, or even of larger single galaxies, but turned out to be adequate for our purpose of obtaining haloes matching the profile of equation 1.

The box was evolved to the present epoch with a standard particle-mesh code, and haloes within the desired range of virial masses were identified in the final state. The corresponding regions within the initial conditions were then resampled using a larger number of particles. We used 4^3 particles per grid zone in the high-resolution region centred on the halo of interest (except for one run with 5^3 particles per zone, to verify that collisional relaxation was negligible). The tidal field was sampled out to a radius of 8 Mpc (using periodic replicas of the original box as needed) with progressively heavier particles at larger distances. Each particle in the high-resolution region thus had a mass of $2.65 \times 10^5 M_\odot$. The high-resolution region was chosen to include those mass elements which in the final state ($z = 0$) of the particle-mesh simulation belonged to the chosen halo (within a local overdensity contour $\delta > 55$, corresponding to a mean enclosed overdensity of about 180 in a spherical collapse model). For our haloes, this region typically contains about $10^{10} M_\odot$, or 40000 particles.

2.2 Initial collapse phase

The resampled initial conditions were evolved for 3.0 Gyr starting from a redshift $z_i = 49$ using a binary tree N -body code. We used a modified version of the code described in Navarro & White (1993), in which the time step selection criterion was made tighter by comparing the third-order Runge-Kutta-Fehlberg terms to the first-order position and velocity increments $|\delta\mathbf{x}|$ and $|\delta\mathbf{v}|$ rather than to the zeroth-order, non-Galilean-invariant positions and velocities $|\mathbf{x}|$ and $|\mathbf{v}|$. For this work we did not make use of the code's built-in Smoothed Particle Hydrodynamics capability, but operated it solely as a gravitational N -body integrator. Each particle was given a gravitational softening length proportional to the cube root of its mass, with high-resolution particles having a softening length of 0.5 kpc, large enough to avoid two-body relaxation effects yet still comfortably smaller than the length scales (such as the 3.0 kpc dark halo core radius) we wish to resolve.

We applied this procedure to 8 of the approximately 20 haloes found within our preferred mass range, then selected three haloes with promising rotation curves for further study. (Although we subjectively deem these rotation curves “promising”, they do not match the observational data particularly well. This fact is illustrated in figure 4 and quantified in table 1, both of which are further described below.) Some scatter in halo properties is expected even in principle, and for want of observational data we do not know where the properties of DDO 154 lie with respect to the ensemble average for objects of that class. In looking for a match to the observed rotation curve we can therefore allow ourselves some reasonable number of tries with different halo realizations.

2.3 Disc growth

At $t = 3.0$ Gyr (except for our first halo, number 99, which was evolved to $t = 3.7$ Gyr; both times were chosen somewhat arbitrarily) we cut a sphere of radius 50 kpc ($\gtrsim 2.5r_{200}$) around the centre of the chosen halo, and applied a Galilean transformation to bring the centre of mass to rest at the origin of coordinates and to align the total angular momentum along the z axis. This was done for practical convenience, as we would otherwise have been forced to incorporate a feedback mechanism to change the position and orientation of the growing disc in response to long-range tidal forces. As it is, we were able to reuse the existing implementation of NEF, in which the disc is symmetric about the z axis and the (x, y) plane. We verified that the density maximum in our simulated haloes does in fact remain close to the origin (to within our target accuracy of ~ 0.5 kpc) during the course of our subsequent runs.

We impose a slowly growing external potential corresponding to a thin axisymmetric disc with surface density $\Sigma(R)$, where R is the radial coordinate within the disc. The corresponding gravitational potential and acceleration were computed on a grid by a Hankel transform technique (Binney & Tremaine 1987, section 2.6.3). A Fast Hankel Transform algorithm (Anderson 1982) allows us to specify essentially arbitrary surface density profiles. In the disc growth phase, however, we only use exponential density dis-

tributions $\Sigma(R) \propto e^{-R/R_d}$ for various values of the scale length R_d .

The disc growth phase lasts 1.5 Gyr, during which the disc gains mass at a constant rate at the expense of the particles in the simulation. We decrease the mass of all the dark matter particles by the same proportion, in such a way that the sum of the masses of halo and disc is conserved. This effectively means that the baryonic disc is formed from a catchment area 50 kpc in radius (this being the size of the sphere we cut out of the previous simulation).

The growth rate is sufficiently slow that the halo responds adiabatically, making the precise history of disc growth irrelevant. Actual galaxy disks are thought to have been assembled slowly (see, e.g., Sommer-Larsen & Vedel (1998)). At the end of the growth phase we allow the system to relax for a period of 0.5 Gyr during which the disc potential is kept constant.

2.4 Disc blow-out

At this time the disc potential is instantaneously changed, in order to mimic the rapid ejection of gas following a burst of star formation. The total disc mass is reduced, and its surface density profile adjusted to match published observational data on DDO 154.

We have found that a profile of the form

$$\Sigma(R) = \Sigma_0 e^{-(\sqrt{R^2 + R_c^2} - R_c)/R_d} \quad (3)$$

with $\Sigma_0 = 5.9M_\odot/\text{pc}^2$, $R_c = 6.1$ kpc and $R_d = 1.0$ kpc provides a very good fit to the HI data of Carignan & Freeman (1988) for a distance of 4 Mpc. The corresponding total HI mass within the radius probed by Carignan & Freeman is $2.63 \times 10^8 M_\odot$.

This only accounts for the gaseous component; for the observed stellar disc remnant we adopt an exponential density profile, which gives a reasonable fit to observations.

In figure 1 we show the run of surface density for the combined gaseous and stellar disc components immediately before (“i” curves) and after (“f” curves) blow-out for two of our simulations. The stellar component is only present in the post-blow-out discs, and only manifests itself as a mass excess in the innermost 1 kpc.

The disc of DDO 154 may contain significant amounts of matter in forms other than the detected HI and stellar components. A rough upper limit can be set by considering the stability of the gaseous disc. According to standard analyses of the problem, beginning with those of Toomre (1964) and of Goldreich & Lynden-Bell (1965), the disc should be stable wherever its surface density lies below a critical value

$$\Sigma_c = \alpha \frac{\kappa c_s}{3.36G} \quad (4)$$

where c_s is the velocity dispersion of the gas, κ the epicyclic frequency, and α a dimensionless constant near unity. We follow Kennicutt (1989) in deriving the epicyclic frequency

$$\kappa = 1.41 \frac{V}{R} \left(1 + \frac{R}{V} \frac{dV}{dR} \right) \quad (5)$$

directly from the observed rotation curve. Figure 2 compares the HI surface density profile (equation [3], solid curve) with the critical surface density Σ_c (equation [4], dashed curve) for $\alpha = 0.7$, $c_s = 3.2$ km/s. These parameter values were

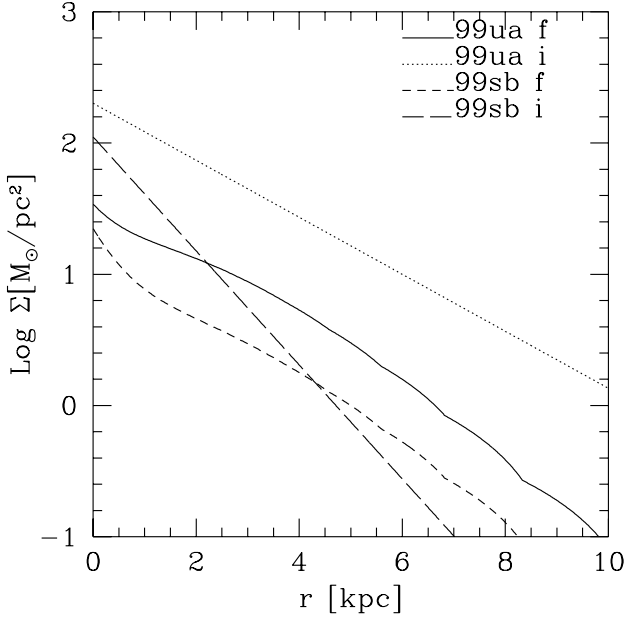


Figure 1. Disc surface density profiles immediately before and after blow-out (labels “i” and “f”, respectively) for two representative simulation runs. The profiles after blow-out include a stellar component in addition to the gas.

chosen to make the surface density profile of equation (3) stable at all radii. They lie at the bottom end of the plausible range of parameters: observed values of the velocity dispersion c_s in disc galaxies typically range between 6 and 10 km/s (unfortunately we could not find in the literature any measurement specific to DDO 154), and the appropriate value for α may also be somewhat larger than 0.7. The observational constraints therefore allow the disc of DDO 154 to be up to at least three times more massive than its observed HI content.

2.5 Free parameters

We allowed ourselves the following adjustments in the parameters of the model:

- (i) varying the disc mass $M_{d,i}$ before blow-out;
- (ii) varying the disc scale length $R_{d,i}$ before blow-out;
- (iii) varying the ratio of total to HI mass in the final disc.

The scale length and mass of the disc before blow-out are not directly observable quantities, and theoretical constraints on them are not very tight, leaving us some leeway in choosing parameters for our models. In general, smaller values of $R_{d,i}$ and larger masses will be more effective in erasing the central cusp. However, it would be remarkable if the initial disc structure were totally unrelated to that of the observed stellar disc remnant. Also, if we assume that the present gaseous disc is mostly made of material that was present in the original disc before blow-out we see that models with very small $R_{d,i}$ tend to be ruled out by there being less angular momentum in the initial disc than in the final one. This is rather different from the assumption made by NEF, that $R_{d,i}$ should be determined by the initial spin parameter $\lambda \sim 0.05$ of the material. One should point

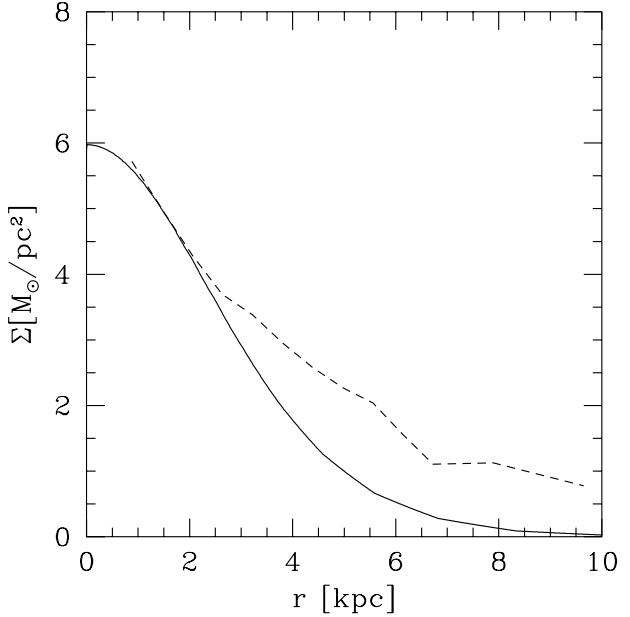


Figure 2. Fit to the surface density profile of the HI component of DDO 154 (solid curve), and critical surface density from equation (4) assuming $\alpha = 0.7$, $c_s = 3.2$ km/s (dashed curve). For these parameters the disc is stable everywhere. Larger values of α and/or c_s lead to larger maximum stable disc masses. Typical observed values of c_s in disk galaxies are between 6 and 10 km/s, allowing for a surface density 2 to 3 times higher than shown in this figure even without invoking the uncertainty in α .

out that the expected distribution of spin parameter values is very broad and that low surface brightness objects (like DDO 154) may very well be so due to a higher degree of rotational support. One way of reconciling these two views would be to assume a large value of $M_{d,i}$ (which would allow $R_{d,i}$ to be decreased), but very large gas masses would conflict with known constraints on the abundance of baryons in the Universe. We adopt an upper limit to the baryonic fraction of 0.3, consistent with observational data on galaxy clusters. (With this choice, nucleosynthesis constraints can also be satisfied for cosmic densities $\Omega \gtrsim 0.3$ with $h = 0.5$.) None of our simulations requires more than this fraction of the mass to be in baryonic form; most require substantially less.

There is an arbitrariness in our choice of cosmological parameters: the $\Omega = 1$, $\Lambda = 0$ standard CDM model is arguably not even the most favoured by observations at the time of this writing. The times at which we start and stop the disk growth were also chosen arbitrarily. Fortunately it appears (NFW) that the structure of virialised haloes is the same across a wide range of cosmologies; accordingly we need not limit ourselves to parameter values (such as the total baryonic mass discussed in the previous paragraph) compatible with $\Omega = 1$ standard CDM. The fact that our haloes were generated using a standard $\Omega = 1$ CDM model should not be viewed as a severe limitation since the choice of cosmology only affects the time of halo formation and the relationship between concentration and mass, but not the internal structure (NFW) or the internal dynamical evolution of the halo after it has collapsed and virialised.

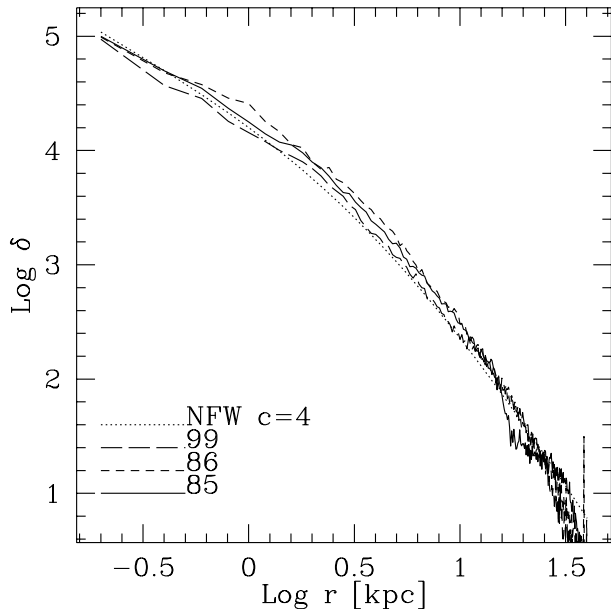


Figure 3. Radial density profiles for the three selected haloes (numbers 85, 86 and 99) at $t = 3.0$ Gyr. The dotted line shows the profile of equation (1) for $c = 4$ and $r_{200} = 18$ kpc.

3 RESULTS

3.1 Initial halo profiles

Figure 3 shows the density profiles of our three chosen haloes before disk growth, and compares them with a fitting NFW profile (dotted line). Figure 4 compares the corresponding rotation curves. The virial mass of our haloes at this time is about $3 \times 10^9 M_{\odot}$. (They were selected to contain about $10^{10} M_{\odot}$ at $z = 0$.) NFW predict a concentration parameter $c \sim 7.8$ at $z = 1.68$, whereas the profiles in our simulations are fitted by $c \sim 4$. (Optimum fits, in which the density in each bin is weighed by the number of particles, actually yield a range of c between 3.2 and 5 and r_s between 3.6 and 5.5 kpc.) The mass scale we are considering here lies outside the range studied by NFW; it is possible that their formula gives poor results when extrapolated. We nonetheless examined four possible sources of error in our simulations: collisional relaxation effects, softened gravity, neglect of small-wavelength seed fluctuations, and finite time steps.

The rate of collisional relaxation is sensitive to the granularity with which the mass is sampled. We repeated one of our runs with 2.35 times the original number of particles, and observed no difference in the resulting profiles up to $t = 4.2$ Gyr, at which point we stopped the higher-resolution run. We feel confident that two-body relaxation is not significantly affecting our results.

We repeated another run with a softening length of 0.1 rather than 0.5 kpc, and again found the profile to be unchanged up to our final simulation time (3.0 Gyr in this instance). This, along with the observation that our characteristic radius $r_s \equiv r_{200}/c$ exceeds the larger of the softening lengths by an order of magnitude, leads us to rule out excessive softening as the cause for our lower-than-expected value of c .

There should be no need to add power down to the par-

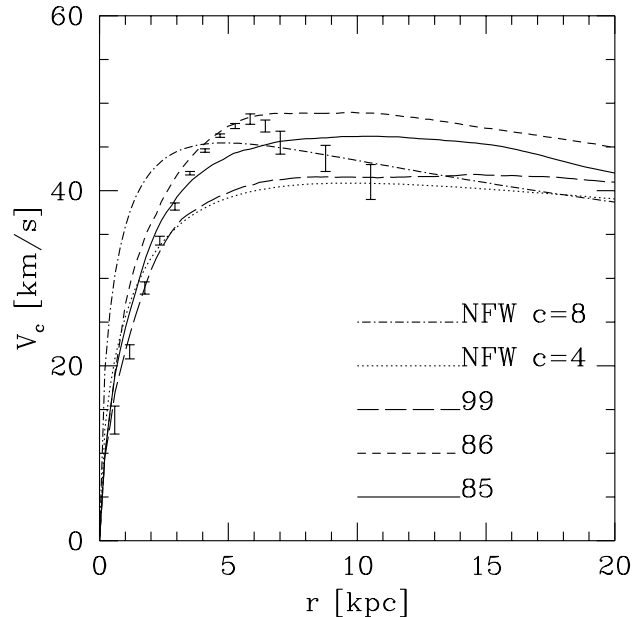


Figure 4. Rotation curves for the three selected haloes at $t = 3.0$ Gyr. Dotted line as in figure 3. Additionally, the dot-dash line shows the rotation curve for an NFW profile with concentration $c = 8$. The vertical error bars represent the observational data on DDO 154.

ticle Nyquist wavenumber. The short-wavelength cutoff for our original 128^3 grid in a $4h^{-1}$ Mpc box corresponds to a characteristic mass of about $1.7 \times 10^7 M_{\odot}$, less than 1% of the virial mass of our haloes. Reproducing the NFW profile is expected to require resolving the collapse of a progenitor with 1% of the final virial mass; our limiting wavelength is just small enough to achieve this. Adding power on even smaller scales would force us to start the simulations at a higher redshift, which in turn would require smaller particle softenings and a larger number of particles to counter collisional relaxation.

Although our changes to the time step selection criterion lead to a more efficient distribution of individual particle time steps, we used a value of the overall tolerance parameter at the high end of the permissible range. We therefore repeated one of our runs with a much smaller tolerance, resulting in a sixteen-fold decrease in time step (from 4×10^6 to 2.5×10^5 years). For the first Gyr, no difference was observed in the density profiles with respect to the run with larger time steps; but starting at a redshift $z \sim 4$ the results began to diverge. The less accurate run evolved towards the shallow, $\rho \propto r^{-1}$ cusp of the NFW profile while the new run maintained a central logarithmic slope much closer to -2 . A run with an intermediate choice of time step gave results in agreement with the smaller-tolerance run, suggesting that results may have converged (or else that they are now limited by a parameter other than the time granularity of the simulation). This seems to confirm the results of Fukushige & Makino (1997), and clearly deserves further investigation. We plan to address this issue in more detail in a forthcoming paper. A second run with initial conditions from one of our other haloes, however, yielded a profile more similar to that of NFW with a concentration $c \sim 8$. (This halo still dis-

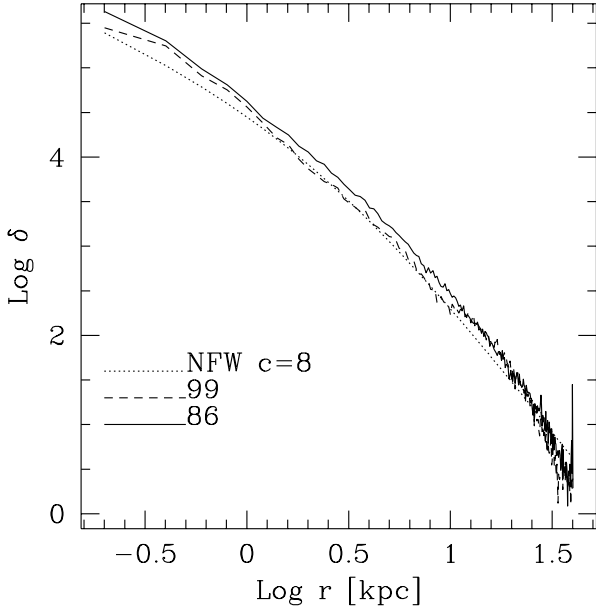


Figure 5. Radial density profiles at $t = 3.0$ Gyr for haloes 86 (solid) and 99 (dashed), integrated with shorter time steps. The dotted line shows the profile of equation 1 for $c = 8$ and $r_{200} = 18$ kpc.

plays a mass excess at small radii, however. Figure 5 shows the density profiles for these two runs.) It appears therefore that at least some haloes are reasonably (but not outstandingly) well fitted by NFW profiles, and that for such haloes the concentration increases only moderately if smaller time steps are used. Moreover, we have no particular reason for favouring $t = 3.0$ Gyr as the time at which the disk began to form: we could equally have picked an earlier time, when the concentration parameter c was smaller (but not *much* smaller, as that turns out to require unreasonably high initial redshifts). Or the true cosmological model could be one in which haloes in this range of masses collapse later, and therefore have smaller c values, than in standard CDM. This is the case in particular for the more favoured Λ -CDM models, in which $\Omega < 1$ and the cosmological constant Λ is of the right magnitude to make the model flat. Open CDM models may also be suitable in this perspective.

We therefore proceed with the analysis of our main series of runs, having no serious grounds for rejecting $c \sim 4$ haloes as a valid starting point for disk growth. For completeness we also performed a few experiments with the more concentrated haloes from the shorter time step integrations. These experiments are computationally much more expensive than our previous ones, and we could only perform a small number of them. We shall briefly discuss the main differences in the results.

3.2 Comparison with observational data

We compare the rotation curves from our simulation runs with the observations of Carignan & Beaulieu (1989), as updated by Carignan & Purton (1997, as reported in BS). For the purpose of estimating the HI mass and the characteristic length scale we place DDO 154 at a distance of 4 Mpc, con-

sistent with photometric data (Carignan & Beaulieu 1989; Hopp & Schulte-Ladbeck 1995).

The published rotation curve data are accompanied by error estimates; we use these in computing a formal χ^2 sum for each of our simulated rotation curves. We caution, however, against taking these χ^2 values too literally. The measure relies on the published uncertainties in the rotation curve, and is therefore dominated by the nominally better data from the inner regions. It also assumes a Gaussian distribution of errors, which may be unrealistic. Finally, it does not take into account the scatter in the numerical models, which is expected to be larger in the inner regions due to the smaller number of particles enclosed; this suggests that one should perhaps give greater weight to the outer part of the rotation curve than implied by the observational uncertainties alone.

As an aid in assessing the overall quality of our fits, we note that an isothermal sphere with a core radius of 3.0 kpc fits the data with $\chi^2 \sim 41$ if we first subtract the gaseous and stellar disc components from the observed rotation curve (assuming that the error bars are not affected). While somewhat better than our best $\chi^2 \sim 88$, these values are significantly poorer than the $\chi^2 \sim 13$ one would expect in a truly outstanding fit with 13 degrees of freedom. The quality of the fits to the rotation curve presented by BS is not directly comparable to ours, since these authors effectively computed an optimal mass distribution for their spheroid component, so that the observed rotation curve is exactly reproduced by construction.

In our fits, we allow ourselves some freedom in rescaling the entire rotation curve by a factor α , chosen optimally for each model. The rescaling factor multiplies both radii and velocities. Masses are implicitly multiplied by α^3 . The transformation leaves dynamical times unchanged. The justification for this rescaling is that we extract haloes from a finite numerical simulation that samples a continuous spectrum of halo properties. Our simulation may not have given us a halo of exactly the right size, and the rescaling is meant to compensate for this. It is naturally essential that the rescaled system remain representative of the underlying halo population. For sufficiently small adjustments a linear rescaling is adequate. We keep the dynamical time constant so that the dynamical age, and hence the internal structure, of each simulated halo is invariant under the rescaling. This may mean that the rescaled halo corresponds to a somewhat different redshift, but since we chose the redshift of disk formation somewhat arbitrarily in the first place this has no adverse impact on the quality of our results. In the ideal case of a singular isothermal sphere, the virial radius at a given redshift is linearly proportional to the circular velocity, just as in our adopted rescaling. (See for example equation 2 of Mo, Mao & White (1998).)

Models for which α differs considerably from unity should be regarded with caution regardless of their nominal χ^2 value: the rescaling applies also to the HI and stellar disc components, which were initially chosen to match observational data with $\alpha = 1$ and no longer agree with these observational data after rescaling by an α very different from unity.

We can also justify rescaling the radial coordinate independently of the circular velocity: both the distance to DDO 154 and the Hubble constant carry uncertainties of at

Table 1. Characteristics of the runs

Run	$M_{d,1}$ [M_{HI}]	$R_{d,1}$ [kpc]	$M_{d,2}$ [M_{HI}]	$M_{H,2}$ [M_{HI}]	$R_{d,2}$ [kpc]	α	$\chi^2_{\nu=13}$	β	γ	$\chi^2_{\nu=12}$
(1)	(2)	(3)	(4)	(5)	(6)	(7)	(8)	(9)	(10)	(11)
85‡						1.06	241	1.59	1.18	143
86‡						0.96	283	1.35	1.05	167
99‡						1.19	179	1.45	1.25	101
99sa	3.5	1	1.2	1	0.5	1.13	152	0.94	1.06	76
99sb	2.7	1	1.2	1	0.5	1.06	89	1.02	1.05	87
99sc	1.8	1	1.2	1	0.5	1.01	136	1.06	1.02	118
99ta	6.4	2	3.2	3	0.5	0.89	326	1.22	0.95	44
99ua	9.6	2	3.2	3	0.5	0.98	165	1.19	1.02	46
85a	9.6	2	3.2	3	0.5	1.00	297	1.35	1.07	60
85b	6.4	2	3.2	3	0.5	0.91	476	1.35	0.99	61
85e	12.8	2	3.2	3	0.5	1.00	230	1.27	1.06	55
86a	9.6	2	3.2	3	0.5	0.97	266	1.28	1.03	61
86b	6.4	2	3.2	3	0.5	0.89	385	1.27	0.96	54
86c	3.5	2	1.2	1	0.5	1.00	188	1.25	1.06	113
86d	1.8	2	1.2	1	0.5	0.94	349	1.45	1.04	119
99Ca‡	9.6	0.5	1.2	1	0.5	1.42	563	1.96	1.41	196
86Ea‡	9.6	0.5	1.2	1	0.5	1.27	338	3.33	1.71	169

least 10–20%. We therefore also present the result of rescaling radii by a factor β and velocities by a factor $\gamma \neq \beta$; the best χ^2 values then become comparable to that for the isothermal sphere fit.

Table 1 summarizes the properties of our main series of runs. Column 1 contains the name of each run; the leading digits identify the halo realisation used as a starting point. Runs marked with a dagger (†) correspond to a higher initial concentration $c \sim 8$ and smaller time steps. Runs marked with a double dagger (‡) represent the dark matter halos before disk growth and removal. Column 2 lists the maximum mass of the exponential disc that has been grown (in units of $M_{\text{HI}} \equiv 2.63 \times 10^8 M_\odot$, the estimated mass of the observed HI disc in DDO 154), and column 3 the scale length of this exponential disc (in kpc). The total mass of the remnant disc after blow-out appears in column 4, and the mass in the HI-like component in column 5. Column 6 shows the exponential scale length of the stellar component of the remnant disc; the mass of this component is given by subtracting column 5 from column 4, and amounts to $5 \times 10^7 M_\odot$ for all the runs presented here. We treat all disc components as having infinite extent. The χ^2 value in column 8 is for $\nu = 13$ degrees of freedom, corresponding to the 14 data points of the observational rotation curve, together with the fact that we allowed ourselves a rescaling of the rotation curve by a factor α (shown in column 7). Columns 9, 10 and 11 correspond to independent rescaling of the radii by a factor β (column 9) and velocities by γ (column 10), yielding $\chi^2_{\nu=12}$ in column 11.

The χ^2 values alone cannot capture all the relevant information about the quality of the fits. We therefore also present plots of the rotation curves for all our runs in figure 6. Each tile in this figure is labelled with the name of the corresponding run from column 1 of table 1. The error bars are centred on the observational data points. The dotted curve represents the raw (unscaled) rotation curve from the simulation run; the dashed curve corresponds to rescaling both r and v by α (table 1, column 7), the solid curve

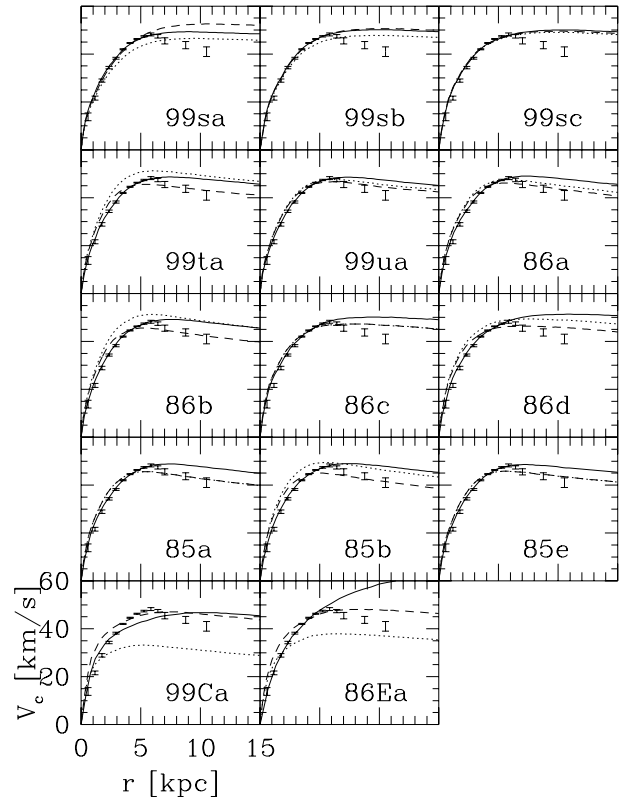


Figure 6. Fits to the rotation curve for the runs listed in table 1. Error bars are centred on the observational data points. Each tile is labelled with the name of the corresponding run. The dotted curve shows the unscaled rotation curve. The dashed curve corresponds to our one-parameter rescaling, the solid curve to our two-parameter rescaling.

to rescaling r by β (column 9) and v by γ (column 10 of table 1).

The quality of the fits appears to be relatively insensitive to the amount of mass loss (compare runs 99sa, 99sb and 99sc; 85a, 85b and 85e; 86a and 86b; 86c and 86d), at least within the range (33% to 75% of the gas mass before blow-out) spanned by our main series of simulations.

It appears difficult to reconcile the observed decline in the circular velocity at large radii without producing some mass excess at small radii. This mass excess can however be contained within reasonable limits. Not unexpectedly, increasing the mass in the remnant gas disk improves the fit to the outer parts of the rotation curve; however, nearly all our models (and certainly all those which provide decent fits to the rising parts of the rotation curve) fall somewhat short of reproducing the observed decline. Given the size of the observational error bars and the idealisations in our model (notably the assumption of instantaneous mass redistribution), however, it is not clear to us that this should be a major source of concern. There is some scatter between our individual halo realizations (compare runs 99ua, 85a, 86a), suggesting that the observations are at least compatible with the overall scenario embodied in our simulations, if not precisely reproduced by the particular halo realizations we tried.

We have also performed a few experiments with more centrally concentrated ($c \sim 8$) initial haloes. (These would be more appropriate models to use if the true cosmology is $\Omega = 1$, $\Lambda = 0$; on the other hand, low- Ω models can produce less concentrated haloes more in line with our $c \sim 4$ runs.) The clear outcome of these runs (99Ca, 86Ea) is that even if we exaggerate the strength of halo pinching by making the disk more massive and more centrally concentrated during the growth phase, we are barely able to produce a central core of the required size, and the overall fit to the observed rotation curve is extremely poor. We must therefore conclude that our scenario only explains the observed rotation curve of DDO 154 if the effective concentration of the dark matter halo was closer to $c = 4$ than to $c = 8$.

Burkert (1995) has pointed out that the core structure of the dark matter halo in DDO 154 appears to be shared by other galaxies in its class, and questioned the ability of the mass ejection hypothesis to produce the fine-tuning that he claims is necessary to turn NFW's one-parameter family of cuspy N -body halo profiles into the different one-parameter family of observed profiles. In this regard we would like to point out that we obtain reasonable fits to the rising part of the rotation curve for a rather wide range of ejected mass fractions; the real challenge is rather to fit the *declining* part of DDO 154's rotation curve. Of the rotation curves in Burkert's (1995) sample, only DDO 154's extends sufficiently far outwards to provide such a stringent test. While his argument about fine-tuning is undoubtedly interesting, we do not find it entirely compelling given the current paucity of observational data.

4 CONCLUSIONS

Our numerical experiments confirm that it is not very easy to give a satisfactory account of the observed rotation curve

of DDO 154 within the framework of a CDM cosmogony. It is, however, possible to obtain a reasonable fit if one assumes

- (i) that sudden mass ejection from the central star-forming regions of the galaxy was responsible for erasing the cusp predicted by CDM models of collisionless gravitational collapse;
- (ii) that the disc of DDO 154 is about three times more massive than implied by its 21 cm H I emission;
- (iii) that the effective halo concentration was low.

We are grateful to Julio Navarro for having made his numerical code available, to Sasha Kashlinsky for early encouragement to look further into this problem, and to Per Rex Christensen for kindly proofreading the manuscript. We also thank the referee for his comments which helped us improve the presentation of this paper. This work was supported by Danmarks Grundforskningsfond through its grant for the establishment of the Theoretical Astrophysics Center.

REFERENCES

- Anderson, W. L., 1982, ACM Trans. Math. Software, 8, 369 (TOMS algorithm 588)
- Binney, J., Tremaine, S., 1987, Galactic dynamics. Princeton University Press
- Burkert, A., 1995, ApJ, 427, L25
- Burkert, A., Silk, J., 1997, ApJ, 488, L55
- Carignan, C., Freeman, K. C., 1988, ApJ, 332, L33
- Carignan, C., Beaulieu, S., 1989, ApJ, 347, 760
- Carignan, C., Purton, C., 1997, ApJ, submitted
- Dubinski, J., Carlberg, R., 1991, ApJ, 378, 496
- Flores, R. A., Primack, J. R., 1994, ApJ, 427, L1
- Fukushige, T., Makino, J., 1997, ApJ, 477, L9
- Goldreich, P., Lynden-Bell, D., 1965, MNRAS, 130, 97
- Hernquist, L., 1990, ApJ, 356, 359
- Hoffman, G. L., Lu, N. Y., Salpeter, E. E., Farhat, B., Lamphier, C., Roos, T., 1993, AJ, 106, 39
- Hopp, U., Schulte-Ladbeck, R. E., 1995, A&AS, 111, 527
- Kennicutt, R. C., 1989, ApJ, 344, 685
- Kravtsov, A.V., Klypin, A.A., Bullock, J.S., Primack, J.R., 1998, ApJ, 502, 48
- Maloney, P., Black, J. H., 1988, ApJ, 325, 389
- Meurer, G.R., Carignan, C., Beaulieu, S.F., Freeman, K.C., 1996, AJ, 111, 1551
- Mo, H.J., Mao, S., White, S.D.M., 1998, MNRAS, 295, 319
- Moore, B., 1994, Nature, 370, 629
- Moore, B., Governato, F., Quinn, T., Stadel, J., Lake, G., 1997, preprint astro-ph/9709051
- Navarro, J. F., White, S. D. M., 1993, MNRAS, 265, 271
- Navarro, J. F., Frenk, C. S., White, S. D. M., 1996, ApJ, 462, 563
- Navarro, J. F., Eke, V. R., Frenk, C. S., 1996, MNRAS, 283, 72
- Navarro, J. F., Frenk, C. S., White, S. D. M., 1997, ApJ, 490, 493
- Sommer-Larsen, J., Vedel, H., 1998, ApJ, submitted
- Splinter, R. J., Melott, A. L., Shandarin, S. F., Suto, Y., 1998, ApJ, 497, 38
- Toomre, A., 1964, ApJ, 139, 1217
- Verter, F., Hodge, P., 1995, ApJ, 446, 616
- van Zee, L., Haynes, M. P., Salzer, J. J., 1997, AJ, 114, 2479